ACS NANO

Cite This: ACS Nano 2018, 12, 12751−12760

www.acsnano.org

ARTICLE

Single Au Atom Doping of Silver Nanoclusters

Marte van der Linden,[†,‡] Arnoldus J. van Bunningen,[¶] Lucia Amidani,[‡] Maarten Bransen,[§] Hebatalla Elnaggar,[†] Pieter Glatzel,[‡] Andries Meijerink,[¶] and Frank M. F. de Groot*[,†]

[†]Inorganic Chemistry and Catalysis, Debye Institute for Nanomaterials Science, Utrecht University, Universiteitslaan 99, 3584 CG Utrecht, The Netherlands

[‡]European Synchrotron Radiation Facility, 71 Avenue des Martyrs, CS 40220, 38043 Grenoble, France

[¶]Condensed Matter and Interfaces, Debye Institute for Nanomaterials Science, Utrecht University, Princetonplein 1, 3584 CC Utrecht, The Netherlands

[§]Soft Condensed Matter, Debye Institute for Nanomaterials Science, Utrecht University, Princetonplein 1, 3584 CC Utrecht, The Netherlands

Supporting Information

ABSTRACT: **Ag_{29} nanoclusters capped with lipoic acid (LA) can be doped with Au. The doped clusters show enhanced stability and increased luminescence efficiency. We attribute the higher quantum yield to an increase in the rate of radiative decay. With mass spectrometry, the Au-doped clusters were found to consist predominantly of $Au_1Ag_{28}(LA)_{12}^{3-}$. The clusters were characterized using X-ray absorption spectroscopy at the Au L_3-edge. Both the extended absorption fine structure (EXAFS) and the near edge structure (XANES) in combination with electronic structure calculations confirm that the Au dopant is preferentially located in the center of the cluster. A useful XANES spectrum can be recorded for lower concentrations, or in shorter time, than the more commonly used EXAFS. This makes XANES a valuable tool for structural characterization.**

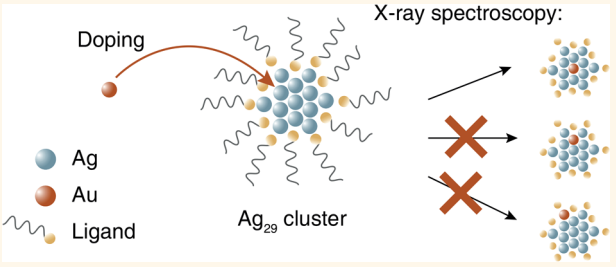

KEYWORDS: *bimetallic nanocluster, doping, Ag_{29}, Au_1Ag_{28}, luminescence, X-ray spectroscopy, structure elucidation*

Thiolate-protected gold and silver nanoclusters are a class of materials with properties such as discrete energy levels, strong luminescence, and potentially atomic monodispersity.[1,2] This is due to their small size, of several hundred atoms or less. The properties of clusters depend on their exact composition and may be affected by changing one atom for an atom of another metal. Bimetallic clusters offer ways to explore fundamental properties of clusters, in addition to a vastly greater range of parameters that can be tuned to obtain clusters with desired properties. The addition of a second metal can drastically enhance the quantum yield,[3] which is of great importance for many potential applications such as sensing[4] and bioimaging.[5] With two metals it is also possible to tune the composition and structure of the cluster surface which may be beneficial for catalysis.[6] The small size and high monodispersity of clusters allows one to understand the changes in optical and electronic properties at the single-atom level.[7] Bimetallic clusters with Au and Ag can be prepared by doping the well-known Au clusters Au_{25}, Au_{38}, and Au_{144} with Ag[8−10] or by introducing Au in Ag clusters such as Ag_{25} and Ag_{44}.[11,12]

We have previously studied Ag clusters with composition $Ag_{29}(LA)_{12}^{3-}$, where LA is the ligand lipoic acid.[13] These clusters are water-soluble, stable for many months, and show bright red luminescence. Recently, Mishra *et al.* showed that doping of these clusters with Au is possible, yielding preferentially Au_1Ag_{28} clusters with enhanced quantum yield.[14] In this work we further study the changes in $Ag_{29}(LA)_{12}^{3-}$ cluster properties upon doping with Au. In agreement with previous work, we find that high concentrations of Au destabilize the cluster, but with a few % Au, a stable bimetallic species is formed, identified as $Au_1Ag_{28}(LA)_{12}^{3-}$ with mass spectrometry. Small amounts of Ag_{29} are still observed, but the contribution of clusters with a higher number of Au atoms is negligible. We further find that the bimetallic cluster has a higher quantum yield than the monometallic cluster, with blueshifts in both emission and absorption spectra. Studies of the luminescence lifetime indicate that doping with Au causes an increase in the rate of radiative decay, which explains the higher luminescence efficiency for a constant nonradiative decay rate.

An important question is the location of the Au atom. Dopants may occupy different sites in clusters, and knowing the location of dopant atoms is necessary to rationalize

Received: October 12, 2018
Accepted: November 20, 2018
Published: November 20, 2018

DOI: 10.1021/acsnano.8b07807
ACS Nano 2018, 12, 12751−12760

changes in cluster properties, such as stability.[15] However, determining which sites are preferentially occupied can be challenging. A number of cluster structures have been determined with X-ray crystallography, and this technique can also be used for bimetallic clusters. An example is the determination of the location of Au atoms in $Au_{12}Ag_{32}$, the bimetallic counterpart of the well-known cluster Ag_{44}.[12] However, growing crystals may be challenging for instance due to the structure and flexibility of the ligand.[16] Even if crystals are obtained, there is no guarantee that all species in the sample crystallize, and for this reason it is possible that only a subpopulation of the sample is probed.[17] An alternative technique is X-ray absorption spectroscopy (XAS). XAS does not require crystalline samples but can be done using disordered solids or solutions. Furthermore, it is element-selective, meaning it can be used to study only the dopant, and purification to remove excess salts or ligands is not necessary. XAS can give information about the electronic structure and local geometry of the absorber, including the nature of ligands, their coordination number, and bond lengths.[18−20] An X-ray absorption spectrum is divided into two regions; the extended X-ray absorption fine structure (EXAFS) and X-ray absorption near edge structure (XANES). EXAFS analysis and interpretation is well-established and can be used to determine bond lengths and the nature of neighboring atoms with high accuracy. It has been successfully used in the study of bimetallic clusters, for example, to determine the preferential position of dopants in $Au_{25}(SR)_{18}$ clusters, where SR indicates the thiolate ligand.[8,21] XANES is less straightforward to interpret and may require comparison to reference spectra of compounds with known structure, together with calculations of spectra for expected structures.[22,23]

In this study, we present XAS at the Au L_3-edge of Au-doped Ag_{29} clusters in solution, using high-energy resolution fluorescence detection (HERFD). Only a narrow band of the emission peak is integrated using a spectrometer with Bragg optics. The integrated bandwidth is narrower than the core-hole lifetime which results in a sharpening of the spectral features compared to XAS recorded in transmission mode or using standard fluorescence detection.[24] Sharper features make it easier to distinguish similar samples. From EXAFS, we find Au−Ag and Au−S coordination numbers that are in good agreement with the Au atom preferentially occupying the central position of the Ag cluster. The low Au concentration of the bimetallic clusters (~30 μM) and requirement for spectra with high signal-to-noise ratio can make EXAFS time-consuming, with a detrimental effect on radiation-sensitive samples. We therefore also recorded XANES. We show that XANES can also be used to identify the dopant location, by combining the experiments with first-principles calculations of Au in different sites. The results confirmed the central position of the Au dopant in the Ag_{29} clusters. A reasonable XANES spectrum could be recorded in 1/50 of the time it took to record EXAFS. Thus, while XANES is less quantitative than EXAFS, it can provide the required information while minimizing exposure of the sample to X-rays.

RESULTS AND DISCUSSION

Optical Properties of Au-Doped Ag Clusters. The bimetallic clusters are made according to the same protocol as Ag_{29} clusters, by replacing some of the $AgNO_3$ solution with $HAuCl_4$ solution. UV−vis absorption spectra of samples with low Au concentrations show blueshifts of all absorption features compared to pure Ag_{29}. A marked increase in luminescence intensity is also observed, along with a slight blueshift of emission wavelength and a decrease in near-infrared (NIR) emission. The reproducibility of the synthesis is not as high as for pure Ag_{29} clusters; therefore, to ensure the accuracy of the observed trend, multiple samples were prepared and emission spectra of all were recorded. Optical properties of bimetallic clusters are summarized in Figure 1,

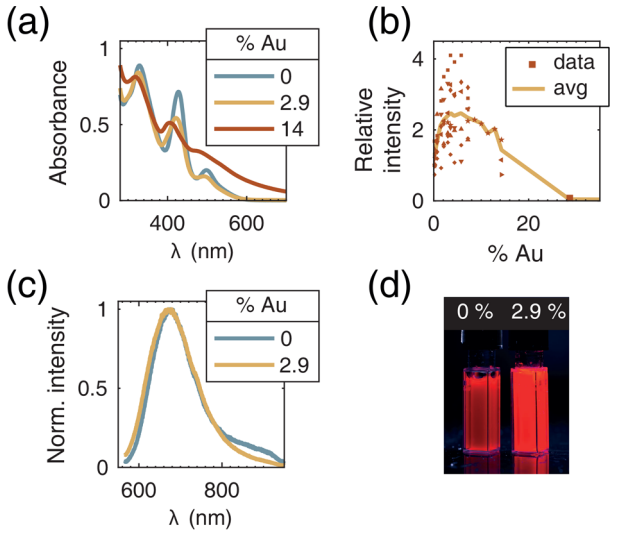

Figure 1. Optical properties of Ag_{29} clusters doped with Au. (a) UV−vis absorption spectra for samples with 0, 2.9, 14% Au. (b) Emission intensity as a function of Au concentration, relative to a pure Ag_{29} sample. Different plot markers represent samples prepared on different days. The yellow line is the average value for all samples. (c) Normalized emission spectra (excited at 400) and (d) photograph of clusters with 0, 2.9% Au under UV light.

and additional spectra can be found in Figure S1. The percentage of gold is given in mol %. Optical properties are in good agreement with what was recently reported by Mishra *et al.*[14] for the same clusters, though no change in shape or position of emission peak was reported in that case.

The quantum yield of clusters with 2.9% Au was determined to be 7.9%, when excited at 485 nm. This is more than 3 times higher than that of pure Ag clusters. Upon excitation at 550 nm, a significantly lower quantum yield of 1.7% is measured. This may be explained by the presence of nonluminescent species which give rise to a background absorption that is more prominent at 550 nm. Additionally, the sample may contain a fraction of pure Ag_{29} clusters, which are predominantly excited at 550 nm due to the blueshift in absorption wavelength upon doping with Au.

There appears to be an optimal Au concentration of around 3−5%, above which the emission intensity decreases again. We attribute the initial increase in intensity and blueshifts in absorption and emission to the incorporation of Au into the Ag_{29} cluster, giving a general cluster formula Au_yAg_{29-y}. The decrease in emission can then be explained if no stable clusters with high y are formed. This is also apparent from the absorption spectra. For 0−7.1% Au, there is a smooth blueshift and decrease in absorbance. At around 14% Au, absorption features are less pronounced, and they disappear entirely at even higher Au concentrations, instead showing only a single broad absorption feature, typical for larger nanoparticles.

DOI: 10.1021/acsnano.8b07807
ACS Nano 2018, 12, 12751−12760

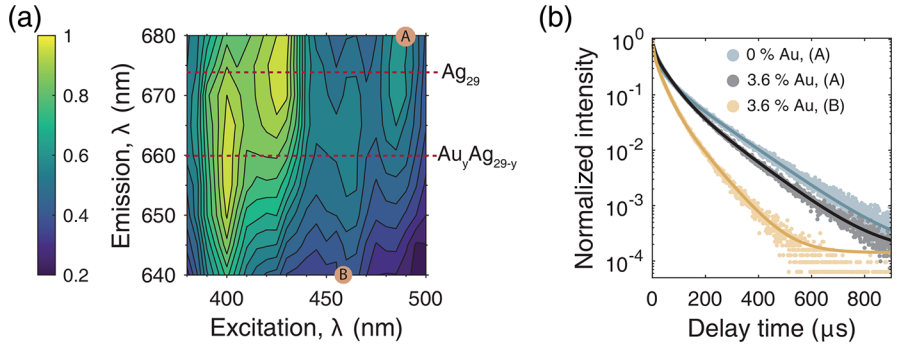

Figure 2. (a) 2D emission and excitation map of clusters with 3.6% Au, recorded at 4 K. The two emission peaks at 675 nm are from Ag_{29}, see Figure S4. (b) Luminescence decay curves at 4 K of clusters with 0 and 3.6% Au. Emission and excitation wavelengths are, respectively, 490 and 680 nm (blue and gray, A) and 460 and 640 nm (yellow, B). A and B thus correspond to mostly Ag_{29} and mostly Au_yAg_{29-y}, respectively. Solid lines are triexponential fits to the data. Luminescence lifetimes at other wavelengths can be found in Figure S5.

The optimal Au concentration lies slightly below that reported by Mishra *et al.* (8%[14]) and far below that found for the organosoluble cluster $Ag_{29}(BDT)_{12}(TPP)_4^{3-}$ (BDT, 1,3-benzenedithiol; TPP, triphenylphosphine)[17] where up to 40% Au was used in the synthesis, resulting in a 26-fold enhancement in quantum yield. Au-doped Ag_{29} with BDT also showed a blueshift in absorption, but the emission spectrum was red-shifted. For $Ag_{25}(SR)_{18}^-$, the incorporation of a single Au atom resulted in a blueshift both in absorption and in emission.[11]

Luminescence Lifetime. The room temperature luminescence lifetime of the clusters was found to decrease with increasing Au doping, from around 4 μs for pure Ag clusters to 2.6 μs for clusters with 14% Au, see Figure S3. As the pure Ag and Au-doped clusters absorb and emit at different wavelengths, we expect to see some variation in the luminescence decay with wavelength as this probes different species. This effect is especially noticeable at 4 K. At low temperatures, the nonradiative decay rate decreases resulting in longer lifetimes and higher luminescence intensity. Blueshifts in absorption and excitation wavelength are also more easily observed as the spectral broadening decreases upon cooling.

A series of emission spectra at different excitation wavelengths was recorded at 4 K and is presented in Figure 2 as a 2D map. For 3.6% Au, the sample shows four features; two at emission wavelength 660 nm and the others at 675 nm. The latter two have excitation wavelengths that are in good agreement with room temperature excitation and absorption spectra of pure Ag clusters. Indeed, a similar 2D map recorded of pure Ag clusters show that these features originate from Ag_{29} (see Figure S4). The two additional features present in the 3.6% Au sample, with excitation wavelengths 400 and 460 nm and emission wavelength 660 nm, thus originate from Au_yAg_{29-y} clusters. As both have the same emission wavelength, it is likely that the sample contains only one other species in addition to Ag_{29}.

Luminescence decay curves of clusters with 3.6% Au at 4 K are shown in Figure 2, for two different emission and excitation wavelengths, together with a measurement of pure Ag clusters. The decay curve of pure Ag_{29} is similar to that of a 3.6% Au sample emitting at 680 nm and excited at 490 nm. These wavelengths correspond to the emission feature assigned to Ag_{29}. When excitation and emission wavelengths of 460 and 640 nm are used, corresponding to the Au_yAg_{29-y} cluster, the decay is significantly faster. The luminescence decay shows multiexponential behavior for bimetallic clusters but also for pure Ag_{29} clusters. This does not necessarily mean there are multiple emitting species. Different environments or conformations of the emitter can influence the rates of decay, leading to an ensemble of emitters with different luminescence lifetimes.[25] There may, for example, be small differences in ligand coordination. While the data may be fitted with multiple exponentials, interpretation of the fit may not be straightforward. Pre-exponential factors and lifetimes are correlated, meaning there may be many possible solutions, which can be hard to distinguish from each other especially if the signal-to-noise ratio is low.[26] Furthermore, the small, finite number of luminescence lifetimes obtained from such a fit may not accurately reflect the shape of the entire distribution actually present in the sample.

The luminescence decay curves at 4 K were fitted with two or three exponentials, with the latter yielding slightly better fits. The triexponential fits are shown in Figure 2, and fit parameters are given in Table S1. The 3.6% Au sample at Au_yAg_{29-y} excitation and emission wavelengths (460 and 640 nm) shows shorter lifetimes and different pre-exponential factors suggesting an overall distribution of faster decay. For further analysis, we calculated the average lifetimes according to $\tau_{avg} = \sum_i I_i t_i / \sum_i I_i$.[25] This equation removes the need for fitting. Pure Ag clusters have an average lifetime of 100 μs. With 3.6% Au, the lifetime at these excitation and emission wavelengths (490 and 680 nm) is 78 μs, while it decreases further to 45 μs at 460 and 640 nm. Average lifetimes at other wavelengths are given in Figure S5. Shorter average lifetimes coincide with wavelengths preferentially probing the Au_yAg_{29-y} clusters. However, even at wavelengths where we expect mostly Ag_{29}, the average lifetime is shorter than for pure Ag clusters, meaning there is probably still some Au_yAg_{29-y} absorbing and emitting due to the overlap of broad emission and excitation peaks. The luminescence spectra of the two types of clusters cannot be separated, and it is therefore not possible to conclusively determine the average lifetime of pure Au_yAg_{29-y}.

Overall, the luminescence of noble metal clusters remains rather poorly understood, and the changes in luminescence behavior upon doping even more so. Ligand-to-metal charge transfer has been proposed as a mechanism for the luminescence of $Au_{25}(SR)_{18}^-$, which showed increased quantum yield with strongly electron-donating ligands.[27] Such a charge transfer mechanism was also suggested for Au clusters with glutathione[28] and monodoped $M_1Ag_{24}(SR)_{18}$ clusters, where the dopant was located in the center of the

DOI: 10.1021/acsnano.8b07807
ACS Nano 2018, 12, 12751−12760

cluster.[29] The dopants (Pd, Ag, Pt, and Au) were found to give different quantum yields which could be related to electron affinity of the dopant and bond lengths from the capping units to the icosahedral core of the clusters. Both factors could influence the ligand-to-metal charge transfer. In contrast, theoretical studies of the luminescence of Au_{25}, Ag_{25}, and Au_1Ag_{24} found that luminescence involves only superatomic orbitals of the cluster and charge-transfer states are not involved.[30,31]

Nevertheless, we can qualitatively explain some of the differences in luminescence behavior between our Ag_{29} and Au_ySAg_{29-y} clusters. Upon doping with Au, the quantum yield increases and the luminescence lifetime decreases. This is in contrast to $Au_1Ag_{24}(SR)_{18}^-$ and Au-doped Ag_{29} clusters capped by BDT.[11,17] In both these cases, a higher quantum yield and a longer lifetime were observed upon incorporation of Au. This suggests different mechanisms may be responsible for the increase in quantum yield upon doping Ag clusters with Au and may depend, for example, on the exact nature of the ligands or structure of the cluster.

The lifetime is the inverse sum of all rates of decay from the excited state, which we group into one overall radiative rate k_r and one overall nonradiative rate k_{nr}. The quantum yield of a system is defined as the ratio between emitted and absorbed photons or, alternatively, the ratio between k_r and $k_r + k_{nr}$. For Au_1Ag_{24} and Au-doped Ag_{29} with BDT, a decrease in nonradiative decay rate is consistent with experimental observations. A decrease in nonradiative decay rate means that a larger fraction will decay *via* the radiative pathway. A recent study of rod-shaped Au_{25} clusters showed that, when they were doped with Ag to give $Ag_{13}Au_{12}$, the quantum yield increased significantly which was attributed to stabilization of the LUMO and enhanced rigidity of the cluster.[32] With increased rigidity, vibrational and rotational motion can be suppressed which decreases the nonradiative decay. This phenomenon is known from organic molecules as aggregation-induced emission[33] and has also been demonstrated for clusters.[34] In contrast, the changes in luminescent behavior we observe upon doping our Ag_{29} clusters with Au are consistent with an increase in radiative decay rate. This results in shorter luminescence lifetimes and an increase in quantum yield. Both our Ag_{29} and Au_ySAg_{29-y} clusters have long microsecond luminescence lifetimes which are characteristic for spin-forbidden transitions.[35] This selection rule can be relaxed through spin−orbit coupling,[36] which is stronger for heavier elements such as Au.[37]

Composition of Bimetallic Clusters. Optical spectroscopy points to one dominant Au-doped cluster species. Electrospray ionization-mass spectrometry (ESI-MS) was used to determine the size of the Au-doped clusters and confirm the successful incorporation of Au. From our previous experiments, it is known that the pure Ag clusters are $Ag_{29}(LA)_{12}^{3-}$ with near atomic monodispersity.[13] The overall charge state of the cluster can be different from 3− due to deprotonation of the ligands, each of which has a carboxylic acid group. Species in the overall 3−, 4−, and 5− charge states are observed. They are deconvoluted in Figure S7. Regardless of the overall charge state, similar spectra are observed. For further analysis, we consider only the species in the overall 5− charge state, as these ion signals are the most intense. This species has two deprotonated ligands. The other 10 ligand carboxylate groups can have either H^+ or Na^+ counterions. This H^+/Na^+ exchange results in multiple species in the same charge state with a mass difference of 22 Da. The full composition of Au-doped Ag_{29} clusters in the overall $z = 5-$ charge state can therefore be written as $[Au_ySAg_{29-y}(LA)_{12}^{3-} - (2 + x)H^+ + x\,Na^+]^{5-}$, where y is between 0 and 29 and x can have values between 0 and 10. The individual isotope signals for each species with different x are not observed but overlap to form a broad peak. The spacing between two adjacent broad peaks is $\Delta m/z$ 4.4, which corresponds to 22 Da in the $z = 5-$ overall charge state. The mass difference upon Ag/Au exchange is 89 Da, which is nearly identical to that of 4 H^+/Na^+ exchanges. This means we expect significant overlap between spectra of Ag_{29} and Au_ySAg_{29-y}.

Figure 3 shows mass spectra of clusters with 0, 2.9, and 7.1% Au as well as theoretical spectra of Ag_{29}, Au_1Ag_{28}, and Au_2Ag_{27}

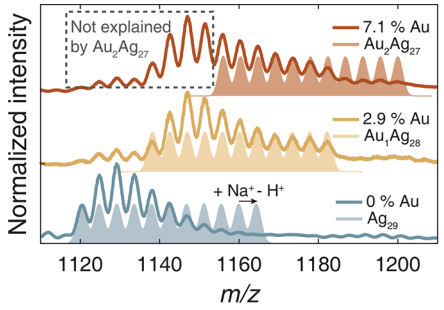

Figure 3. Mass spectra, in the $z = 5$ overall charge state, of samples with 0, 2.9, and 7.1% Au, which corresponds to average compositions of Ag_{29}, $Au_{0.8}Ag_{28.2}$, and $Au_{2.1}Ag_{26.9}$, respectively. Theoretical spectra of Ag_{29}, Au_1Ag_{28} and Au_2Ag_{27} are shown in lighter colors for comparison. Note that the most intense ion signals of the 7.1% Au sample are not explained by the average composition Au_2Ag_{27}. Theoretical spectra are calculated for the compositions $[Au_ySAg_{29-y}(LA)_{12}^{3-} - (2 + x)\,H^+ + xNa^+]^{5-}$, where x is between 0 and 10. The spacing between peaks corresponds to H^+/Na^+ exchange, and individual isotope signals are not resolved. See also Figure S6.

with all possible H^+/Na^+ exchanges (different values of x). Spectra of a larger range of samples are shown in Figure S6. It is clear from the spectra that the sample with 2.9% Au contains mostly Au_1Ag_{28}. There is a small amount of Ag_{29} visible (first four ion signals, m/z 1120−1143) and no contribution from Au_2Ag_{27} (as seen by the lack of intense ion signals in the region m/z 1187−1200). For samples with 7.1% Au (on average 2.1 Au atoms per cluster), we again observe mostly Au_1Ag_{28} with minor contributions of Ag_{29} and Au_2Ag_{27}. Even with 14.3% Au, the cluster Au_1Ag_{28} dominates the spectrum, despite the average composition being Au_4Ag_{25} (see Figure S6). There appears to be a preference for monodoped clusters, as previously observed by Mishra *et al.*[14]

To estimate concentrations of each cluster in a sample is challenging due to the overlapping ion signals. Experimental spectra are therefore fitted to a weighted sum of theoretical spectra, for each combination of x and y with the assumption that each cluster has the same distribution of Na^+ adduct peaks. Full details of the fitting model can be found in the Supporting Information and the results are summarized in Figure S8. We find that all samples show a higher concentration of Au_1Ag_{28} relative to Ag_{29} and Au_2Ag_{27} than would be expected if Au was distributed randomly across all clusters. Note that a preference for monodoped clusters during synthesis may be further enhanced by high stability of Au_1Ag_{28} compared to Ag_{29} and Au_2Ag_{27} during purification prior to

DOI: 10.1021/acsnano.8b07807
ACS Nano 2018, 12, 12751−12760

mass spectrometry measurements or during cluster ionization. The less stable clusters suffer more degradation, and the resulting species may remain undetected, much like degraded Ag_{29}.[13]

Postsynthesis Modification. The standard synthesis protocol involves addition of metal salts to a solution of LA (made soluble by reduction), followed by reduction to form clusters. Both the pure Ag and the bimetallic clusters appear to follow the same synthesis pathway: after reduction, the solution turns black, then slowly lightens during the next hours until it is a reddish orange color. A second way to prepare the bimetallic clusters is by postsynthesis modification of pure Ag clusters. This is done by addition of $HAuCl_4$ to a previously prepared Ag_{29} sample, followed by reduction with $NaBH_4$. The sample then darkens and turns brown, but after several hours of stirring the orange color returns. UV−vis absorption spectra show that the final sample has similar absorption features as Au-doped Ag clusters prepared according to the standard procedure (Figure S9). When only $HAuCl_4$ (or only $NaBH_4$) is added, there is only a slight change in absorbance but no shift in absorption wavelength, proving that both reagents are needed for successful conversion.

Based on the redox potentials of $AuCl_4^-$/Au and Ag^+/Ag, one would expect a redox reaction to occur and Au to be incorporated into the cluster in a galvanic exchange reaction when only Au^{3+} is added. This was observed in the synthesis of thiolate-protected Ag_7Au_6 clusters, which were made from Ag_7 and Ag_8 by adding $AuCl_4^-$.[38] However, the small size of the clusters and the presence of ligands can influence such reactions. An anti- galvanic exchange reaction was observed for $Au_{25}(SC_2H_4Ph)_{18}$, which reacted with Ag^+ to form bimetallic species such as Ag_2Au_{23} and Ag_3Au_{22},[39] although the reaction did not occur when glutathione was used as a ligand.[40] Interestingly, Bootharaju *et al.* found that the only way to prepare monodisperse $Au_1Ag_{24}(SR)_{18}^-$ clusters was by galvanic exchange, using $Ag_{25}(SR)_{18}^-$ and Au^{3+}.[11] A direct synthesis from Ag and Au salts gave instead a range of alloy clusters $Au_yAg_{25-y}(SR)_{18}^-$, as also demonstrated in a number of other studies.[41,42]

Au-doped Ag_{29} clusters prepared *via* postsynthesis modification also show a preference for monodoped clusters. Due to the two reduction steps with $NaBH_4$, the Na^+ concentration is higher than usual in this sample giving intense Na^+ adduct signals (see Figure S10). The preference for monodoping with gold, both *via* a direct synthesis and postsynthesis modification, appears to be specific for Ag_{29} with LA. For BDT-capped Ag_{29}, direct synthesis with Au yielded a distribution of different compositions with 1−7 Au atoms, although one that shows a preference for clusters with a low number of dopants.[17] Doping with Pt yielded only a small fraction of Pt_1Ag_{28} when direct synthesis was done.[43] For Au-doped Ag_{25}, direct synthesis also resulted in a mixture of clusters with different number of Au atoms, while the monodoped cluster was only obtained *via* postsynthesis modification.[11]

Stability of Bimetallic Clusters. We further find that doping with gold increases the stability of the Ag_{29} clusters. This was demonstrated by exposing samples with 0, 2.9, and 7.1% Au to UV-light, as shown in Figure S11. Over time, the characteristic absorption features disappear for all samples, but bleaching is fastest for the pure Ag clusters. The pure Ag sample showed only a slight blueshift of the absorption features (3 nm). With 2.9 and 7.1% Au, the blueshifts were 13 and 6 nm, respectively. The large blueshift observed for the 2.9% Au sample can be explained by the different stabilities of the species present in this sample; Ag_{29} and Au_1Ag_{28}. The pure Ag clusters are bleached more rapidly than Au_1Ag_{28}. Thus, over time, the relative concentration of Au_1Ag_{28} increases and its blueshifted absorption features dominate the spectrum. The difference in stability between pure Ag and Au-doped clusters was also observed when 0 and 7.1% Au clusters were exposed to heat by placing samples on a hot plate for several hours.

An increase in stability was also found for BDT-capped Ag_{29} upon doping with Au or Pt.[17,43] Similarly, Pt_1Au_{24},[44] Pd_1Au_{24},[45] and Au_1Ag_{24}[11] were found to be more stable than their monometallic counterparts. Alloying Au_{25} with Cu, on the other hand, reduced the stability of the clusters.[46] This is attributed to the small size of Cu (atomic radius 1.28 Å) compared to Au (1.44 Å), which leads to distortions of the structure. It has also been observed that Au−Ag alloy clusters are less stable than pure Au clusters.[9] This can be explained by bond strengths, which in bulk are found to be Au−Au > Au−Ag > Ag−Ag.[47] Conversely, doping a Ag cluster with a small amount of Au will introduce a number of strong Ag− Au bonds.

Location of the Au Atom. The bimetallic clusters were further studied with X-ray absorption spectroscopy to determine the position of the Au atom in the bimetallic cluster. EXAFS of a 2.9% Au sample was recorded without any additional purification or concentration. Mass spectrometry and optical spectroscopy do not exclude the presence of small Au−LA complexes or clusters in the samples after synthesis, and the lack of purification ensures all Au species are taken into account. Due to the low Au concentration in the samples (30 μM), multiple EXAFS spectra were recorded over a total time period of 4 h. The cluster solution was placed in a liquid jet setup so that the same fraction of sample was not continuously exposed to X-rays. Despite the use of this setup, radiation damage was observed, resulting in a color change of the sample from orange to brown and a disappearance of prominent UV−vis absorption features (see Figure S13). The radiation damage, and its effect on XAS, will be discussed in more detail later.

For a first analysis, the radiation damage was ignored and all EXAFS scans were averaged. The averaged spectrum was fitted to two scattering paths, one Au−S and one Au−Ag. The spectrum is shown together with the fit in Figure 4. The results of the fit are given in Table 1. The Au−Ag coordination number, 7.8, is significantly higher than the average Ag−Ag coordination number in pure Ag_{29}, which is around 3.[48] Clearly, the Au atom does not occupy a random position in the doped cluster. We assume that the clusters have a similar structure as $Ag_{29}(BDT)_{12}(TPP)_4^{3-}$, which is a reasonable assumption as cluster composition and optical properties are similar.[48] The structure of this cluster is shown in Figure S12. There are four different sites the Au atom may occupy; in the center of the icosahedron (*center*), on the outer icosahedral positions (*ico*), in the capping units, bound to LA (*shell*), and on the external positions bound only to phosphines (*ext*). Note that the LA-capped clusters do not have the phosphines, so these sites may not exist with the same coordination geometry. The lack of phosphines may also distort the rest of the surface, giving slightly different coordination numbers for *shell* sites. Expected coordination numbers can be found in Table 2.

DOI: 10.1021/acsnano.8b07807
ACS Nano 2018, 12, 12751−12760

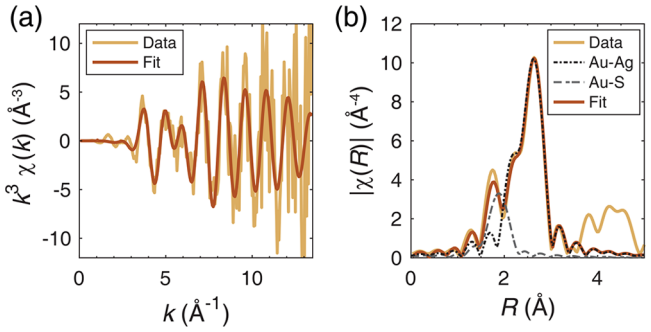

Figure 4. EXAFS of Au-doped Ag_{29} clusters solution in (a) k and (b) R-space. The fit was done using scattering paths Au−S and Au−Ag of Au_1Ag_{28} using the structure of Ag_{29} with BDT,[48] where the Au atom occupies one of the outer positions of the icosahedron (*ico*). The contributions of each path are also shown in part b. The results of the fit are given in Table 1. For this figure, all EXAFS scans are averaged together (even though we observe some radiation damage).

Table 1. Structural Parameters of Au-Doped Ag29 Clusters from EXAFS Analysis[a]

parameter	Au−S	Au−Ag
CN	1.16 ± 0.61	7.82 ± 1.55
R (Å)	2.29 ± 0.04	2.78 ± 0.01
σ^2 (10^{-3} Å^2)	5.05 ± 5.46	8.98 ± 1.42
E_0 (eV)	3.8 ± 5.8	4.2 ± 1.3

[a]CN is the coordination number, R the bond length, σ^2 the Debye−Waller factor, and E_0 the energy shift. The fit is shown in Figure 4. For this fit, the R-factor = 0.024 and reduced χ^2 = 48. The amplitude reduction factor is not taken into account (i.e, S_0^2 = 1) for the values in the table. From fitting of the Au reference, it was estimated to be between 0.95 and 1.0.

Table 2. Expected Coordination Numbers (CN) of Au in Different Sites, Assuming the Clusters Have the Same Structure As $Ag_{29}(BDT)_{12}(TPP)_4$[3−48a]

site	CN (Au−S)	CN (Au−Ag)
center	0	12
ico	1	6
shell	3	2[b]
ext	3	0

[a]Only Au−Ag bonds shorter than 3 Å are considered, except where explicitly noted. [b]These bonds are slightly longer, around 3.1.

The Au−Ag coordination number of 7.8 can only be explained if a significant fraction of Au occupies a *center* or *ico* position. Furthermore, we observe an Au−S bond length of 2.29 Å, which is shorter than the 2.46 Å Ag−S bond present in pure Ag_{29} clusters.[48] It is, however, consistent with typical bond lengths of Au−S bonds in Au clusters[49,50] and gold thiolates.[51] Thus, Au in *shell* or *ext* sites would cause a significant surface distortion. The observed Au−S bonds may be present in Au clusters or Au-thiolate complexes, rather than in Au_1Ag_{28}.

From color changes, and by comparing UV−vis absorption spectra before and after EXAFS, it is clear that there is radiation damage. Radiation damage is ubiquitous and may seriously affect the recorded spectrum and thus the interpretation of the experimental data.[52] It is of great importance to determine the effect of radiation damage on the X-ray spectrum and at which time scale this occurs, as this determines how long a sample may be measured before changes in the electronic structure of the absorber occur. The X-ray beam may induce chemical changes of the sample at sites that are far from the X-ray absorber.[53] If these changes do not measurably modify the electronic structure around the absorber, the sample is considered intact with respect to the X-ray spectroscopy measurements. Therefore, the best probe to study radiation damage in XAS is XAS itself. To monitor the radiation damage, XANES was recorded every 25 min between EXAFS scans. There are minor changes in XANES over time, most notably a decrease in whiteline intensity (see Figure S13). The change is observed already within 1 h and stabilizes after 2 h. The first half of the scans, 0−2 h, represents a relatively undamaged sample, while the effect of radiation damage is more severe in the 2−4 h range.

It is possible to get a better understanding of the damage process and thus by extension the undamaged sample, by comparing the first and second half of the EXAFS scans (Figure S14). Due to the lower signal-to-noise ratio when only half the scans were considered, fitting was more challenging and in some cases required the use of constraints for parameters of the Au−S scattering path. The first half of the scans could also be successfully fitted using only the Au−Ag scattering path. In the first half of the EXAFS scans, the Au−Ag coordination number is around 10, while in the second half it decreases to around 7. In contrast, the Au−S coordination number shows a slight increase to around 1.5 in the second half. Radiation damage thus either causes the Au to migrate to the surface of the cluster or results in cluster degradation yielding gold thiolate species. The high Au−Ag coordination number before extensive radiation damage shows a strong preference for Au in the *center* site, in the middle of the cluster.

EXAFS requires high-quality spectra with high signal-to-noise ratio, which may take a long time to record. XANES presents an intriguing addition to EXAFS for the analysis of bimetallic clusters to determine dopant location. It has lower detection limits than EXAFS which allows for the study of dilute samples. It is less critical for the spectra to have high signal-to-noise ratio, making it beneficial for the study of radiation-sensitive compounds. XANES is sensitive to the number and identity of ligands as well as that of next-nearest neighbors. A downside is that the analysis is less straightforward than for EXAFS.

Au L_3-edge HERFD-XANES was recorded between EXAFS scans to monitor radiation damage, but we can also use these XANES scans for further analysis. It took only 5 min to record a spectrum with good signal-to-noise ratio, as shown in Figure 5. The spectrum shows a strong whiteline and a number of well-resolved postedge features. The spectrum was compared to first-principles calculations of Au in possible sites of Ag_{29} (see Figure S12 for the used structure). Mass spectrometry identified Au_1Ag_{28} as the major species in the sample with 2.9% Au, so this composition was used for the calculations. The agreement with the calculated spectrum of Au_1Ag_{28} is excellent when Au occupies the *center* position. Both EXAFS and XANES lead to the same conclusion. However, radiation damage is significantly less severe for XANES. As discussed previously, radiation damage causes a decrease in whiteline intensity, as shown in Figure S13. The 5 min HERFD-XANES spectrum presented in Figure 5 was recorded well within the time scale for the damage, which becomes noticeable after 30−50 min. During the 5 min it took to record XANES, no

DOI: 10.1021/acsnano.8b07807
ACS Nano 2018, 12, 12751−12760

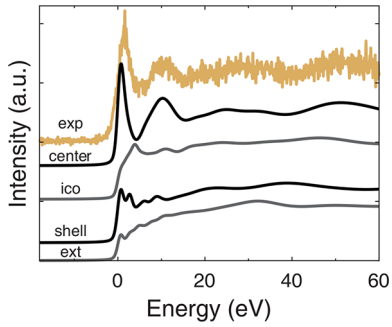

Figure 5. Experimental Au L_3-edge HERFD-XANES of Au-doped Ag_{29} clusters (2.9% Au), together with results of FDMNES calculations for an Au atom in each of the four possible locations in Ag_{29}.

changes are observed in the spectral features. Thus, XANES measurements in combination with calculations identify the location of Au in the cluster with considerable less required measurement time than EXAFS. This allows to mitigate the problem of radiation damage considerably.

The spectrum in Figure 5 was recorded using the same resolution as for EXAFS (1.8 eV). The resolution could be improved further to 0.5 eV, but this also reduced the intensity of the signal. No novel features were observed with the improved resolution (Figure S15).

As a further demonstration of the usefulness of XANES, we also calculated spectra of Au doped in another silver nanocluster, $Ag_{25}(SR)_{18}$, which has an icosahedral core surrounded by six $Ag_2(SR)_3$ units.[54] Spectra of Au occupying different positions in this cluster (Figure S17) are markedly different. Furthermore, spectra of Au in the center of Ag_{25} and Ag_{29} are comparable, probably due to the similarity in structure of the inner icosahedral core in both clusters. It may therefore be unnecessary to know the exact structure of the cluster and arrangement of ligands on the surface to gain useful knowledge about the location of dopants. Samples containing a mixture of doped clusters could be analyzed using linear combination analysis, principal component analysis, or more advanced fitting procedures, using experimental or calculated spectra of each species.[23]

A preference for monodoping in the center of clusters is also observed for Pd[15] and Pt[21] in Au_{25}. The monodoped Au_1Ag_{24} cluster, prepared *via* postsynthesis modification, also has the Au atom in the center of the cluster.[11] Monodoping can be rationalized when a cluster doped in the *center* position exhibits a significantly higher stability than a cluster with dopants in other locations, or an undoped or multidoped cluster. The Au−Ag bond is stronger than the Ag−Ag bond.[47] When an Au atom occupies the *center* position in Ag_{29}, the number of Au−Ag bonds is maximized, which explains the preference for *center* doping. In Au clusters, alloying with Ag results in Ag at *ico* sites in Au_{25}[8,42] and similar sites in Au_{144}.[55,56] Doping Ag_{44} clusters with Au has been shown to result in clusters with composition $Au_{12}Ag_{32}$. This cluster consists of a hollow icosahedral core (12 Au atoms) surrounded by a dodecahedral shell (20 Ag atoms) and six $Ag_2(SR)_5$ capping units.[12] The Au atoms do not occupy the capping units nor the metal shell immediately below, just as for our Au_1Ag_{28} clusters. Clearly, *ico* sites are more favorably occupied by Ag than Au. We further propose that Au atoms cannot go into the capping layer of Ag_{29} (*shell* and *ext* sites) as this would result in significant structural distortions and thus a lower stability due to the change in bond length from Ag−S to Au−S. Indeed, changes in capping unit metal are rare in AgAu alloy clusters.[57] In BDT-capped Ag_{29}, it was found that also the *ext* sites could be replaced with Au,[17] but the presence of phosphines may help stabilize these doped clusters due to the strong Au−P bond.[58,59]

CONCLUSIONS

The introduction of dopants is a promising method for tuning nanocluster properties. In this article, the effects of introducing Au into $Ag_{29}(LA)_{12}^{3-}$ clusters were investigated. Au atoms could be incorporated both *via* direct synthesis or by postsynthesis modification, with both methods yielding clusters with similar properties. Doping with Au resulted in enhanced stability to heat and UV-light. The optical properties of the cluster were also affected, with blueshifts in both absorption and emission spectra. We further observed an increase in quantum yield by a factor of 3−4 and a decrease in luminescence lifetime from 4 to 2.6 μs. Together, these observations indicate an increase in radiative decay rate for the doped cluster which is explained by lifting the spin-selection rule by enhanced spin−orbit coupling upon doping with the heavier Au. The optical properties suggest the presence of a single type of Au-doped Ag_{29} species. Electrospray ionization mass spectrometry measurements confirmed that doped samples contain predominantly $Au_1Ag_{28}(LA)_{12}^{3-}$. X-ray absorption spectroscopy was used to determine that the Au atom occupies the central position in the cluster. We show that XANES may be used in addition to EXAFS for the identification of dopant locations. We propose that clusters with Au atoms located on surface sites would cause structural distortions and therefore be less stable. This may explain the strong preference for monodoped species.

METHODS

Chemicals. $AgNO_3$ (laboratory reagent grade) was obtained from Fisher Scientific. $NaBH_4$ (99%), (±)-α-lipoic acid (≥99%), methanol (≥99.9%), and $HAuCl_4{\cdot}3H_2O$ (≥99.9%) were purchased from Sigma-Aldrich. 1-Butanol (99.5%) was obtained from Acros. Water was of Milli-Q quality, purified using a Millipore Direct-Q 3 water purification system. 4-(Dicyanomethylene)-2-methyl-6-(4-dimethylaminostyryl)-4H-pyran (DCM dye) was obtained from Exciton.

Synthesis. The synthesis of the Ag clusters is based on a protocol by Adhikari *et al.*[60] and the same as our previously reported protocol for the synthesis of Ag_{29} clusters.[13] Bimetallic clusters are prepared using the same general protocol. In total, 19 mg of lipoic acid (92 μmol) and 7 mg of $NaBH_4$ (185 μmol) were placed in a 40 or 20 mL glass vial with 14 mL of water. This was stirred (using a magnetic stirring bar) until all LA had dissolved. Next, 25 mM $AgNO_3$ and $HAuCl_4{\cdot}3H_2O$ solutions were added, with a combined volume of 700 μL (corresponding to 17.5 μmol in total). For many of the experiments, 20 μL of $HAuCl_4$ solution was used, corresponding to 2.9% Au. The $AgNO_3$ solution was always added first, and the addition of $HAuCl_4{\cdot}3H_2O$ was followed by 10 mg of $NaBH_4$ (264 μmol) in 2 mL of water. The vial was wrapped in aluminum foil to minimize the exposure of the clusters to light, and stirring was continued overnight. The synthesis was performed at room temperature.

Postsynthesis modification was done by preparing Ag_{29} according to the standard procedure. After a day, 25 mM $HAuCl_4{\cdot}3H_2O$ solution was added to a total Au concentration of 2.9 or 7.1%, followed by the addition of 10 mg of $NaBH_4$ in solid form. The solution was then stirred overnight. All samples were stored in the dark at room temperature

Optical Spectroscopy. UV−vis spectra were recorded using a PerkinElmer Lambda 950, a PerkinElmer Lambda 40, or a Varian

DOI: 10.1021/acsnano.8b07807
ACS Nano 2018, 12, 12751−12760

Cary 50 spectrometer. Room temperature emission spectra were recorded with a Jasco FP8300 spectrofluorometer or a 450 W xenon lamp and a Spex 1680 (0.22 m) spectrofluorometer for excitation and an Acton Research SpectraPro 300i monochromator with a liquid N_2 cooled Princeton Instruments CCD camera for detection of emission spectra. The CCD camera was equipped with a 150 lines/mm grating blazed at 800 nm. Emission spectra were corrected for the spectral response of the equipment. Emission and excitation spectra at 4 K were recorded using an Edinburgh Instrument FLS920 spectrofluorometer, with a Hamamatsu R928 photomultiplier as detector and a 450 W xenon lamp as the excitation source. The setup was equipped with an Oxford Instruments cryostat for liquid helium. Room temperature luminescence lifetimes were recorded using a Hamamatsu R928 photomultiplier with a time-correlated single photon counting card (TimeHarp 260 PC, PicoQuant), and Nd:YAG laser (third harmonic at 355 nm) pumped Optical Parametric Oscillator (OPO, Opolette HE 355-II, Opotec Inc.) operating at 500 nm giving ~10 ns pulses or a 441 nm pulsed diode laser (Edinburgh Instruments EPL-445, 65 ps pulses) as the excitation source. At low temperature, luminescence lifetimes were recorded with a slightly modified version of this setup. A Hamamatsu H7422 photomultiplier was used as detector, and the OPO laser operating at 420, 460, or 490 nm was used as the excitation source. For optical spectroscopy measurements, the clusters solution was diluted 4−10× with water; the dilution was the same when comparing different samples for the same experiment.

Quantum Yield Determination. The quantum yield of pure Ag and Au-doped Ag clusters was determined using DCM dye in ethanol as reference. A Varian Cary 50 spectrometer was used to record UV−vis absorption spectra. Emission spectra were recorded on a Jasco FP8300 spectrofluorometer. The excitation wavelengths used were 485 and 550 nm. Clusters and DCM dye were diluted with water or ethanol to prepare five samples with absorbance ≲0.1 at 485 nm. The integrated emission intensity of each spectrum scales linearly with the absorbance at 485 nm (see Figure S2); the slopes of the lines are proportional to the quantum yield. The quantum yield of DCM dye in ethanol is 43.5%.[61] The quantum yield of the clusters can be calculated according to eq 1,

$$\Phi = \Phi_R \frac{m}{m_R} \frac{n^2}{n_R^2} \quad (1)$$

where m is the slope from Figure S2, n is the solvent refractive index, and Φ is the quantum yield. In each case, the subscript R refers to the reference dye. Values for the solvent refractive index are n = 1.33336 and n_R = 1.3611 for water and ethanol, respectively.[62]

Stability Tests. The stability of clusters solution to UV-light was tested by placing samples by a UVP UVGL-58 hand-held UV-lamp (365 nm excitation wavelength, 6 W) while minimizing the influence of other light sources. UV−vis absorption spectra were recorded at regular intervals. To test the stability against heat, pure Ag clusters and Au-doped Ag clusters were placed together on a hot plate at 80 °C for 6 h.

Mass Spectrometry. MS measurements were performed in negative ion mode using an electrospray ionization-time-of-flight (ESI-TOF) instrument (LC-T; Micromass, Manchester, U.K.) equipped with a Z-spray nanoelectrospray ionization source. A nano ESI quadrupole TOF instrument (Micromass, Manchester, U.K.) was used for tandem mass spectrometric analysis. Needles were made from borosilicate glass capillaries (Kwik-Fil, World Precision Instruments, Sarasota, FL) on a P-97 puller (Sutter Instruments, Novato, CA), coated with a thin gold layer by using an Edwards Scancoat (Edwards Laboratories, Milpitas, CA) six Pirani 501 sputter coater. After purification, the sample was sprayed into the mass spectrometer. The applied voltage on the needle was between 1200 and 1100 V, and the sample cone voltage was varied between −7 and 0 V. All spectra were mass calibrated in negative ion mode, using an aqueous solution of phosphoric acid (0.1% v/v). All samples were purified using 1-butanol to extract water, containing excess ligands and other possible contaminants, in several steps until the clusters sediment, after which they are washed with a small amount of methanol and redispersed in water. Details are given in the Supporting Information. Theoretical spectra were calculated using ChemCalc[63] for the compositions $[Au_yAg_{29-y}(LA)_{12}^{3-} - (2 + x)\ H^+ + xNa^+]^{5-}$, where x is between 0 and 10.

X-ray Spectroscopy. Au L_3-edge XAS (11.92 keV) was recorded at beamline ID26 at the European Synchrotron Radiation Facility. The incident beam was selected using the (111) reflection from a double Si crystal monochromator. The spectrometer was equipped with a set of five Ge(555) analyzer crystals (R = 1000 mm, r = 50 mm) to record high-energy resolution fluorescence detected (HERFD) XAS. The 2p3d fluorescence channel was monitored ($L\alpha_1$, 9.71 keV) for all experiments. The overall energy bandwidth was ~1.8 eV, which is well below the core-hole lifetime broadening of 5.54 eV.[64] A further improvement of the energy resolution to 0.5 eV was obtained by using the (311) reflection of the monochromator, removing one of the analyzer crystals (as this particular crystal had a slightly lower quality than the others) and by placing a mask with radius 25 mm in front of each of the four remaining analyzer crystals. Only XANES was recorded with these settings, as the higher resolution also results in a lower intensity (these XANES spectra are shown in the Supporting Information). A liquid jet setup was used to minimize radiation damage. The sample (2.9% Au, prepared at 5× the standard scale) was placed in a vial from which liquid was pumped through a capillary to form a free-standing liquid jet which was placed in the focus of the beam. Below the jet, the liquid was collected and returned to the vial.

EXAFS Analysis. EXAFS analysis was done using VIPER[65] and the Athena and Artemis software packages.[66] Scattering phases and amplitudes were calculated using FEFF for $Ag_{29}(BDT)_{12}(TPP)_4$,[48] with TPP (triphenylphosphine) ligands removed and BDT (1,3-benzenedithiol) replaced by LA. A geometry optimization of this structure was done in Avogadro,[67] keeping Ag and S atoms frozen, to ensure reasonable C−C and C−H bond lengths and angles. One of the Ag atoms in the icosahedral shell was replaced by Au to model an average environment with both Au−Ag and Au−S paths that were used in the fit. Typical fit parameters were k = 3.0−12.0 Å^{-1}, R = 1.15−3.3 Å, using a Hanning window (dk = 1 Å^{-1}) for the Fourier transformation. Fitting was done using k = 3 weighting in VIPER and k = 1, 2, 3 weighting in Artemis. The amplitude reduction factor S^2 was not explicitly taken into account during fitting (*i.e.*, S^2 = 1 was used). However, from fitting a reference Au sample, it may be estimated to be between 0.95 and 1.0.

XANES Analysis. The experimental spectrum was compared to calculations using FDMNES.[68] The structure of the cluster was taken from that of Ag_{29} protected with BDT,[48] modified in the same way as described above for EXAFS analysis. The FDMNES calculations were done for an Au atom in each inequivalent site in $Au_1Ag_{28}(LA)_{12}$. A radius of 6 Å was used for each calculation. This corresponds to the distance from the central atom to the outer Ag atoms. Atomic potentials, Fermi level, and charge transfer were calculated self-consistently, and the finite difference method was used to calculate potentials.[69,70] Spin−orbit interactions were included in the calculation for core and valence state with the keyword *relativism*. The spectra were convoluted to apply an energy-dependent broadening, using default parameters (an arctangent function). The width of the core-hole was decreased to 0.50 eV and further broadened with a 1.0 eV Gaussian, to better match the experimental data. Additional calculations were done of an Au atom in different sites of $Ag_{25}(SR)_{18}^-$, using the experimentally determined structure without any modifications.[54]

ASSOCIATED CONTENT

Supporting Information

The Supporting Information is available free of charge on the ACS Publications website at DOI: 10.1021/acsnano.8b07807.

Additional UV−vis absorption and emission spectra at room temperature and 4 K, additional luminescence lifetimes, tests of cluster stability, additional mass spectra

DOI: 10.1021/acsnano.8b07807
ACS Nano 2018, 12, 12751−12760

and details of sample purification, postsynthesis modification of Ag clusters, effect of radiation damage during XAS, XANES spectra with 0.5 eV resolution, and additional XANES calculations (PDF)

AUTHOR INFORMATION

Corresponding Author

*E-mail: F.M.F.deGroot@uu.nl.

ORCID

Marte van der Linden: 0000-0002-4085-0320
Arnoldus J. van Bunningen: 0000-0001-5162-7258
Lucia Amidani: 0000-0003-2234-4173
Maarten Bransen: 0000-0002-4002-5291
Pieter Glatzel: 0000-0001-6532-8144
Andries Meijerink: 0000-0003-3573-9289
Frank M. F. de Groot: 0000-0002-1340-2186

Notes

The authors declare no competing financial interest.

ACKNOWLEDGMENTS

The authors thank A. Barendregt for help with mass spectrometry measurements. The ESRF is thanked for providing beamtime (Proposal CH4593). This work was financially supported by the Debye Graduate Programme (NWO Project 022.004.016), and ESRF Graduate Programme. The mass spectrometry research was performed within the framework of NWO and supported by the large scale proteomics facility Proteins@Work (Project 184.032.201) embedded in The Netherlands Proteomics Centre.

REFERENCES

(1) Jin, R.; Zeng, C.; Zhou, M.; Chen, Y. Atomically Precise Colloidal Metal Nanoclusters and Nanoparticles: Fundamentals and Opportunities. *Chem. Rev.* **2016**, *116*, 10346−10413.

(2) Chakraborty, I.; Pradeep, T. Atomically Precise Clusters of Noble Metals: Emerging Link between Atoms and Nanoparticles. *Chem. Rev.* **2017**, *117*, 8208−8271.

(3) Wang, S.; Meng, X.; Das, A.; Li, T.; Song, Y.; Cao, T.; Zhu, X.; Zhu, M.; Jin, R. A 200-fold Quantum Yield Boost in the Photoluminescence of Silver-Doped Ag_x Au_{25-x} nanoclusters: The 13th Silver Atom Matters. *Angew. Chem., Int. Ed.* **2014**, *53*, 2376−2380.

(4) Zhou, T.-y.; Lin, L.-p.; Rong, M.-c.; Jiang, Y.-q.; Chen, X. Silver-Gold Alloy Nanoclusters as a Fluorescence-Enhanced Probe for Aluminum Ion Sensing. *Anal. Chem.* **2013**, *85*, 9839−9844.

(5) Le Guével, X.; Trouillet, V.; Spies, C.; Li, K.; Laaksonen, T.; Auerbach, D.; Jung, G.; Schneider, M. High Photostability and Enhanced Fluorescence of Gold Nanoclusters by Silver Doping. *Nanoscale* **2012**, *4*, 7624−7631.

(6) Wang, S.; Jin, S.; Yang, S.; Chen, S.; Song, Y.; Zhang, J.; Zhu, M. Total Structure Determination of Surface Doping $[Ag_{46}Au_{24}(SR)_{32}]$-$(BPh_4)_2$ Nanocluster and its StructureTelated Catalytic Property. *Sci. Adv.* **2015**, *1*, No. e1500441.

(7) Jin, R.; Nobusada, K. Doping and Alloying in Atomically Precise Gold Nanoparticles. *Nano Res.* **2014**, *7*, 285−300.

(8) Yamazoe, S.; Kurashige, W.; Nobusada, K.; Negishi, Y.; Tsukuda, T. Preferential Location of Coinage Metal Dopants (M = Ag or Cu) in $[Au_{25-x}M_x(SC_2H_4Ph)_{18}]^-$ ($x \sim 1$) As Determined by Extended X-ray Absorption Fine Structure and Density Functional Theory Calculations. *J. Phys. Chem. C* **2014**, *118*, 25284−25290.

(9) Kumara, C.; Dass, A. AuAg alloy Nanomolecules with 38 Metal Atoms. *Nanoscale* **2012**, *4*, 4084−4086.

(10) Kumara, C.; Dass, A. $(AuAg)_{144}(SR)_{60}$ Alloy Nanomolecules. *Nanoscale* **2011**, *3*, 3064−3067.

(11) Bootharaju, M. S.; Joshi, C. P.; Parida, M. R.; Mohammed, O. F.; Bakr, O. M. Templated Atom-Precise Galvanic Synthesis and Structure Elucidation of a $[Ag_{24}Au(SR)_{18}]^-$ Nanocluster. *Angew. Chem., Int. Ed.* **2016**, *55*, 922−926.

(12) Yang, H.; Wang, Y.; Huang, H.; Gell, L.; Lehtovaara, L.; Malola, S.; Häkkinen, H.; Zheng, N. All-Thiol-Stabilized Ag_{44} and $Au_{12}Ag_{32}$ Nanoparticles with Single-Crystal Structures. *Nat. Commun.* **2013**, *4*, 2422.

(13) van der Linden, M.; Barendregt, A.; van Bunningen, A. J.; Chin, P. T. K.; Thies-Weesie, D. M.; de Groot, F. M. F.; Meijerink, A. Characterisation, Degradation and Regeneration of Luminescent Ag_{29} Clusters in Solution. *Nanoscale* **2016**, *8*, 19901−19909.

(14) Mishra, D.; Lobodin, V.; Zhang, C.; Aldeek, F.; Lochner, E.; Mattoussi, H. Gold-Doped Silver Nanoclusters with Enhanced Photophysical Properties. *Phys. Chem. Chem. Phys.* **2018**, *20*, 12992−13007.

(15) Tofanelli, M. A.; Ni, T. W.; Phillips, B. D.; Ackerson, C. J. Crystal Structure of the $PdAu_{24}(SR)_{18}^0$ Superatom. *Inorg. Chem.* **2016**, *55*, 999−1001.

(16) Das, A.; Liu, C.; Byun, H. Y.; Nobusada, K.; Zhao, S.; Rosi, N.; Jin, R. Structure Determination of $[Au_{18}(SR)_{14}]$. *Angew. Chem., Int. Ed.* **2015**, *54*, 3140−3144.

(17) Soldan, G.; Aljuhani, M. A.; Bootharaju, M. S.; AbdulHalim, L. G.; Parida, M. R.; Emwas, A.-H.; Mohammed, O. F.; Bakr, O. M. Gold Doping of Silver Nanoclusters: A 26-Fold Enhancement in the Luminescence Quantum Yield. *Angew. Chem., Int. Ed.* **2016**, *55*, 5749−5753.

(18) Newville, M. Fundamentals of XAFS. *Rev. Mineral. Geochem.* **2014**, *78*, 33−74.

(19) Penner-Hahn, J. E. In *Comprehensive Coordination Chemistry II*, 2nd ed.; McCleverty, J. A., Meyer, T. J., Eds.; Elsevier, 2003; pp 159−186.

(20) Zhang, P. X-ray Spectroscopy of Gold-Thiolate Nanoclusters. *J. Phys. Chem. C* **2014**, *118*, 25291−25299.

(21) Christensen, S. L.; MacDonald, M. A.; Chatt, A.; Zhang, P.; Qian, H.; Jin, R. Dopant Location, Local Structure, and Electronic Properties of $Au_{24}Pt(SR)_{18}$ Nanoclusters. *J. Phys. Chem. C* **2012**, *116*, 26932−26937.

(22) Manceau, A.; Lemouchi, C.; Rovezzi, M.; Lanson, M.; Glatzel, P.; Nagy, K. L.; Gautier-Luneau, I.; Joly, Y.; Enescu, M. Structure, Bonding, and Stability of Mercury Complexes with Thiolate and Thioether Ligands from High-Resolution XANES Spectroscopy and First-Principles Calculations. *Inorg. Chem.* **2015**, *54*, 11776−11791.

(23) Timoshenko, J.; Shivhare, A.; Scott, R. W. J.; Lu, D.; Frenkel, A. I. Solving Local Structure Around Dopants in Metal Nanoparticles with Ab Initio Modeling of X-ray Absorption Near Edge Structure. *Phys. Chem. Chem. Phys.* **2016**, *18*, 19621−19630.

(24) Glatzel, P.; Weng, T.-C.; Kvashnina, K.; Swarbrick, J.; Sikora, M.; Gallo, E.; Smolentsev, N.; Mori, R. A. Reflections on Hard X-ray Photon-In/Photon-Out Spectroscopy for Electronic Structure Studies. *J. Electron Spectrosc. Relat. Phenom.* **2013**, *188*, 17−25.

(25) Lakowicz, J. R. *Principles of Fluorescence Spectroscopy*, 3rd ed.; Springer Science: New York, 2006; pp 97−155.

(26) Grinvald, A.; Steinberg, I. Z. On the Analysis of Fluorescence Decay Kinetics by the Method of Least-Squares. *Anal. Biochem.* **1974**, *59*, 583−598.

(27) Wu, Z.; Jin, R. On the Ligand's Role in the Fluorescence of Gold Nanoclusters. *Nano Lett.* **2010**, *10*, 2568−2573.

(28) Stamplecoskie, K. G.; Chen, Y.-S.; Kamat, P. V. Excited-State Behavior of Luminescent Glutathione-Protected Gold Clusters. *J. Phys. Chem. C* **2014**, *118*, 1370−1376.

(29) Liu, X.; Yuan, J.; Yao, C.; Chen, J.; Li, L.; Bao, X.; Yang, J.; Wu, Z. Crystal and Solution Photoluminescence of $MAg_{24}(SR)_{18}$ (M = Ag/Pd/Pt/Au) Nanoclusters and Some Implications for the Photoluminescence Mechanisms. *J. Phys. Chem. C* **2017**, *121*, 13848−13853.

(30) Weerawardene, K. L. D. M.; Aikens, C. M. Theoretical Insights into the Origin of Photoluminescence of $Au_{25}(SR)_{18}^-$ Nanoparticles. *J. Am. Chem. Soc.* **2016**, *138*, 11202−11210.

DOI: 10.1021/acsnano.8b07807
ACS Nano 2018, 12, 12751−12760

(31) Weerawardene, K. L. D. M.; Aikens, C. M. Origin of Photoluminescence of $Ag_{25}(SR)_{18}^-$ Nanoparticles: Ligand and Doping Effect. *J. Phys. Chem. C* **2018**, *122*, 2440−2447.
(32) Zhou, M.; Zhong, J.; Wang, S.; Guo, Q.; Zhu, M.; Pei, Y.; Xia, A. Ultrafast Relaxation Dynamics of Luminescent Rod-Shaped, Silver-Doped Ag_x Au_{25-x} Clusters. *J. Phys. Chem. C* **2015**, *119*, 18790−18797.
(33) Hong, Y.; Lam, J. W. Y.; Tang, B. Z. Aggregation-Induced Emission: Phenomenon, Mechanism and Applications. *Chem. Commun.* **2009**, *0*, 4332−4353.
(34) Goswami, N.; Yao, Q.; Luo, Z.; Li, J.; Chen, T.; Xie, J. Luminescent Metal Nanoclusters with Aggregation-Induced Emission. *J. Phys. Chem. Lett.* **2016**, *7*, 962−975.
(35) Velázquez, J. J.; Tikhomirov, V. K.; Chibotaru, L. F.; Cuong, N. T.; Kuznetsov, A. S.; Rodríguez, V. D.; Nguyen, M. T.; Moshchalkov, V. V. Energy Level Diagram and Kinetics of Luminescence of Ag Nanoclusters Dispersed in a Glass Host. *Opt. Express* **2012**, *20*, 13582−13591.
(36) Marian, C. M. Spin-Orbit Coupling and Intersystem Crossing in Molecules. *WIREs Comput. Mol. Sci.* **2012**, *2*, 187−203.
(37) Atkins, P.; de Paula, J.; Keeler, J. *Atkins' Physical Chemistry*, 11th ed.; Oxford University Press: Oxford, 2018; pp 324−370.
(38) Udayabhaskararao, T.; Sun, Y.; Goswami, N.; Pal, S. K.; Balasubramanian, K.; Pradeep, T. Ag_7Au_6: A 13-Atom Alloy Quantum Cluster. *Angew. Chem., Int. Ed.* **2012**, *51*, 2155−2159.
(39) Wu, Z. Anti-Galvanic Reduction of Thiolate-Protected Gold and Silver Nanoparticles. *Angew. Chem., Int. Ed.* **2012**, *51*, 2934−2938.
(40) Wu, Z.; Wang, M.; Yang, J.; Zheng, X.; Cai, W.; Meng, G.; Qian, H.; Wang, H.; Jin, R. Well-Defined Nanoclusters as Fluorescent Nanosensors: a Case Study on $Au_{25}(SG)_{18}$. *Small* **2012**, *8*, 2028−2035.
(41) Dou, X.; Yuan, X.; Yao, Q.; Luo, Z.; Zheng, K.; Xie, J. Facile Synthesis of Water-Soluble Au_{25-x} Ag_x Nanoclusters Protected by Mono- and Bi-Thiolate Ligands. *Chem. Commun.* **2014**, *50*, 7459−7462.
(42) Kumara, C.; Aikens, C. M.; Dass, A. X-ray Crystal Structure and Theoretical Analysis of Au_{25-x} Ag_x $(SCH_2CH_2Ph)_{18}^-$ Alloy. *J. Phys. Chem. Lett.* **2014**, *5*, 461−466.
(43) Bootharaju, M. S.; Kozlov, S. M.; Cao, Z.; Harb, M.; Parida, M. R.; Hedhili, M. N.; Mohammed, O. F.; Bakr, O. M.; Cavallo, L.; Basset, J.-M. Direct versus Ligand-Exchange Synthesis of $[PtAg_{28}(BDT)_{12}(TPP)_4]^{4-}$ Nanoclusters: Effect of a Single-Atom Dopant on the Optoelectronic and Chemical Properties. *Nanoscale* **2017**, *9*, 9529−9536.
(44) Qian, H.; Jiang, D.-e.; Li, G.; Gayathri, C.; Das, A.; Gil, R. R.; Jin, R. Monoplatinum Doping of Gold Nanoclusters and Catalytic Application. *J. Am. Chem. Soc.* **2012**, *134*, 16159−16162.
(45) Negishi, Y.; Kurashige, W.; Niihori, Y.; Iwasa, T.; Nobusada, K. Isolation, Structure, and Stability of a Dodecanethiolate-Protected Pd_1Au_{24} Cluster. *Phys. Chem. Chem. Phys.* **2010**, *12*, 6219−6225.
(46) Gottlieb, E.; Qian, H.; Jin, R. Atomic-Level Alloying and De-alloying in Doped Gold Nanoparticles. *Chem. - Eur. J.* **2013**, *19*, 4238−4243.
(47) Ferrando, R.; Jellinek, J.; Johnston, R. L. Nanoalloys: From Theory to Applications of Alloy Clusters and Nanoparticles. *Chem. Rev.* **2008**, *108*, 845−910.
(48) AbdulHalim, L. G.; Bootharaju, M. S.; Tang, Q.; Del Gobbo, S.; AbdulHalim, R. G.; Eddaoudi, M.; Jiang, D.-e.; Bakr, O. M. $Ag_{29}(BDT)_{12}(TPP)_4$: A Tetravalent Nanocluster. *J. Am. Chem. Soc.* **2015**, *137*, 11970−11975.
(49) Yamazoe, S.; Takano, S.; Kurashige, W.; Yokoyama, T.; Nitta, K.; Negishi, Y.; Tsukuda, T. Hierarchy of Bond Stiffnesses within Icosahedral-Based Gold Clusters Protected by Thiolates. *Nat. Commun.* **2016**, *7*, 10414.
(50) MacDonald, M. A.; Chevrier, D. M.; Zhang, P.; Qian, H.; Jin, R. The Structure and Bonding of $Au_{25}(SR)_{18}$ Nanoclusters from EXAFS: the Interplay of Metallic and Molecular Behavior. *J. Phys. Chem. C* **2011**, *115*, 15282−15287.
(51) Elder, R. C.; Ludwig, K.; Cooper, J. N.; Eidsness, M. K. EXAFS and WAXS Structure Determination for an Antiarthritic Drug, Sodium Gold(I) Thiomalate. *J. Am. Chem. Soc.* **1985**, *107*, 5024−5025.
(52) Yano, J.; Kern, J.; Irrgang, K.-D.; Latimer, M. J.; Bergmann, U.; Glatzel, P.; Pushkar, Y.; Biesiadka, J.; Loll, B.; Sauer, K.; Messinger, J.; Zouni, A.; Yachandra, V. K. X-ray Damage to the Mn_4Ca Complex in Single Crystals of Photosystem II: A Case Study for Metalloprotein Crystallography. *Proc. Natl. Acad. Sci. U. S. A.* **2005**, *102*, 12047−12052.
(53) Ramallo-López, J. M.; Giovanetti, L. J.; Vicentin, F. C.; Requejo, F. G. XANES Study of the Radiation Damage on Alkanethiolates-Capped Au Nanoparticles. *J. Phys.: Conf. Ser.* **2013**, *430*, 012034.
(54) Joshi, C. P.; Bootharaju, M. S.; Alhilaly, M. J.; Bakr, O. M. $[Ag_{25}(SR)_{18}]^-$: The "Golden" Silver Nanoparticle. *J. Am. Chem. Soc.* **2015**, *137*, 11578−11581.
(55) Malola, S.; Häkkinen, H. Electronic Structure and Bonding of Icosahedral Core-Shell Gold-Silver Nanoalloy Custers Au_{144-x} Ag_x $(SR)_{60}$. *J. Phys. Chem. Lett.* **2011**, *2*, 2316−2321.
(56) Malola, S.; Lehtovaara, L.; Häkkinen, H. TDDFT Analysis of Optical Properties of Thiol Monolayer-Protected Gold and Intermetallic Silver-Gold $Au_{144}(SR)_{60}$ and $Au_{84}Ag_{60}(SR)_{60}$ Clusters. *J. Phys. Chem. C* **2014**, *118*, 20002−20008.
(57) Fan, J.; Song, Y.; Chai, J.; Yang, S.; Chen, T.; Rao, B.; Yu, H.; Zhu, M. The Solely Motif-Doped $Au_{36-x}Ag_x$ $(SPh-tBu)_{24}$ $(x = 1 - 8)$ Nanoclusters: X-ray Crystal Structure and Optical Properties. *Nanoscale* **2016**, *8*, 15317−15322.
(58) Juarez-Mosqueda, R.; Malola, S.; Häkkinen, H. Stability, Electronic Structure, and Optical Properties of Protected Gold-Doped Silver $Ag_{29-x}Au_x$ $(x = 0 - 5)$ Nanoclusters. *Phys. Chem. Chem. Phys.* **2017**, *19*, 13868−13874.
(59) Schwerdtfeger, P.; Hermann, H. L.; Schmidbaur, H. Stability of the Gold(I)-Phosphine Bond. A Comparison with other Group 11 Elements. *Inorg. Chem.* **2003**, *42*, 1334−1342.
(60) Adhikari, B.; Banerjee, A. Facile Synthesis of Water-Soluble Fluorescent Silver Nanoclusters and Hg(II) Sensing. *Chem. Mater.* **2010**, *22*, 4364−4371.
(61) Rurack, K.; Spieles, M. Fluorescence Quantum Yields of a Series of Red and Near-Infrared Dyes Emitting at 600−1000 nm. *Anal. Chem.* **2011**, *83*, 1232−1242.
(62) Rumble, J. R., Ed. *CRC Handbook of Chemistry and Physics*; 2017; www.hbcponline.com.
(63) Patiny, L.; Borel, A. ChemCalc: A Building Block for Tomorrow's Chemical Infrastructure. *J. Chem. Inf. Model.* **2013**, *53*, 1223−1228.
(64) Campbell, J. L.; Papp, T. Widths of the Atomic K-N7 Levels. *At. Data Nucl. Data Tables* **2001**, *77*, 1−56.
(65) Klementev, K. V. Extraction of the Fine Structure from X-ray Absorption Spectra. *J. Phys. D: Appl. Phys.* **2001**, *34*, 209−217.
(66) Ravel, B.; Newville, M. ATHENA, ARTEMIS, HEPHAESTUS: Data Analysis for X-ray Absorption Spectroscopy Using IFEFFIT. *J. Synchrotron Radiat.* **2005**, *12*, 537−541.
(67) Hanwell, M. D.; Curtis, D. E.; Lonie, D. C.; Vandermeersch, T.; Zurek, E.; Hutchison, G. R. Avogadro: An Advanced Semantic Chemical Editor, Visualization, and Analysis Platform. *J. Cheminf.* **2012**, *4*, 17.
(68) Bunau, O.; Joly, Y. Self-Consistent Aspects of X-ray Absorption Calculations. *J. Phys.: Condens. Matter* **2009**, *21*, 345501.
(69) Amestoy, P. R.; Guermouche, A.; L'Excellent, J. Y.; Pralet, S. Hybrid Scheduling for the Parallel Solution of Linear Systems. *Parallel Comput.* **2006**, *32*, 136−156.
(70) Guda, S. A.; Guda, A. A.; Soldatov, M. A.; Lomachenko, K. A.; Bugaev, A. L.; Lamberti, C.; Gawelda, W.; Bressler, C.; Smolentsev, G.; Soldatov, A. V.; et al. Optimized Finite Difference Method for the Full-Potential XANES Simulations: Application to Molecular Adsorption Geometries in MOFs and Metal-Ligand Intersystem Crossing Transients. *J. Chem. Theory Comput.* **2015**, *11*, 4512−4521.

DOI: 10.1021/acsnano.8b07807
ACS Nano 2018, 12, 12751−12760